Check for updates

RESEARCH ARTICLE



Alzheimer's disease and its co-pathologies: Implications for hippocampal degeneration, cognitive decline, and the role of APOF £4

Klara Gawor¹ Sam Verrept¹ Geethika Arekatla² David Wouters³ David Wouters Alicja Ronisz¹ Moritz Hecht⁴ Celeste Laureyssen^{5,6} Helena Ver Donck¹ Bas Lahaije¹ | Simona Ospitalieri¹ | Mathieu Vandenbulcke⁷ | Markus Otto^{8,9} | Christine A. F. von Arnim^{8,10} Estifanos Ghebremedhin¹¹ Bernard Hanseeuw¹² Rik Vandenberghe^{13,14} Matthew Blaschko¹⁵ Alejandro Sifrim³ Kristel Sleegers^{5,6} Dietmar Rudolf Thal^{1,16} Sandra O. Tomé¹

Correspondence

Dietmar Thal, Department of Imaging and Pathology, KU Leuven, Herestraat 49, B-3000 Leuven, Belgium.

Email: dietmar.thal@kuleuven.be

Abstract

INTRODUCTION: In neurodegenerative dementias, the co-occurrence and interaction of amyloid β peptide (A β), tau pathology, and other pathological lesions confound their individual contributions to neurodegeneration and their modulation by risk factors.

Kristel Sleegers, Dietmar Rudolf Thal, and Sandra O. Tomé contributed equally and are listed in alphabetical order.

This is an open access article under the terms of the Creative Commons Attribution-NonCommercial-NoDerivs License, which permits use and distribution in any medium, provided the original work is properly cited, the use is non-commercial and no modifications or adaptations are made. © 2025 The Author(s). Alzheimer's & Dementia published by Wiley Periodicals LLC on behalf of Alzheimer's Association.

¹Department of Imaging and Pathology, Laboratory of Neuropathology, KU Leuven, Leuven, Belgium

²Department of Neuroscience, Laboratory of Neurobiology, KU Leuven, Leuven, Belgium

³Department of Human Genetics, Laboratory of Multi-omic Integrative Bioinformatics, KU Leuven, Leuven, Belgium

⁴Laboratory of Neuropathology, Institute of Pathology, Ulm University, Ulm, Germany

⁵Complex Genetics of Alzheimer's Disease Group, VIB Center for Molecular Neurology, VIB, Antwerp, Belgium

⁶Department of Biomedical Sciences, University of Antwerp, Antwerp, Belgium

 $^{^7}$ Department of Neuroscience, Laboratory for Translational Neuropsychiatry, KU Leuven, Leuven, Belgium

⁸Department of Neurology, Ulm University, Ulm, Germany

⁹Department of Neurology, University of Halle, Halle, Germany

 $^{^{10}}$ Department of Geriatrics, University Medical Center Göttingen, Göttingen, Germany

¹¹Institute of Anatomy, Johann Wolfgang Goethe University, Frankfurt, Germany

¹²Institute of Neuroscience, UCLouvain, Brussels, Belgium

¹³Department of Neurology, UZ Leuven, Leuven, Belgium

¹⁴Department of Neurosciences, Laboratory for Cognitive Neurology, KU Leuven, Leuven, Belgium

¹⁵Department of Electrical Engineering, Processing Speech and Images, KU Leuven, Leuven, Belgium

¹⁶Department of Pathology, UZ Leuven, Leuven, Belgium

Funding information

Fonds Wetenschappelijk Onderzoek, Grant/Award Numbers: G0F8516N. G065721N, G024925N [DRT], 1225725N [SOT]; KU Leuven Onderzoeksraad, Grant/Award Numbers: C14/17/107, C14/22/132, C3/20/057 [DRT], PDMT2/21/069 [SOT]; Alzheimer's Association, Grant/Award Numbers: 22-AAIIA-963171 [DRT], AARF-24-1300693 [SOT]; Deutsche Forschungsgemeinschaft, Grant/Award Numbers: TH-624-4-1, TH-624-4-2, TH-624-6-1 [DRT], SFB1279 [MO]; Alzheimer Forschung Initiative, Grant/Award Numbers: #10810, #13803 [DRT]; BrightFocus Foundation, Grant/Award Number: A2022019F[SOT]; German Federal Ministry of Education and Research. Grant/Award Number: FTLDc01GI1007A [MO]; Boehringer Ingelheim UIm University BioCenter, Grant/Award Number: D.5009 [MO]; EU Moodmarker program, Grant/Award Number: 01EW2008 [MO]; Thierry Latran Foundation, Grant/Award Numbers: D.2468, D.2468 [MO]; Foundation of the State of Baden-Württemberg, Grant/Award Number: D.3830 [MO]; BonaRes, Grant/Award Number: 01GI1007A [MO]; Roux Program of the Martin Luther University Halle-Wittenberg, Grant/Award Number: [MO]; EU Joint Programme-Neurodegenerative Diseases network Genfi-Prox, Grant/Award Number: 01ED2008A [MO]

METHODS: We analyzed 480 *post mortem* human brains (ages 50–99) using regression and structural equation models to assess the relationships among $A\beta$, tau, limbic-predominant age-related TDP-43 encephalopathy neuropathological changes (LATE-NC), α -synuclein, other age-related lesions, and apolipoprotein E (*APOE*) ε 4, as well as their effects on CA1 neuronal density, brain weight, and cognitive status.

RESULTS: A β , tau, LATE-NC, and amygdala-predominant α -synuclein pathology were mutually interdependent. Tau was the strongest predictor of global neurodegeneration, while LATE-NC primarily, but not exclusively, affected hippocampal neuron loss. Small vessel disease correlated with both LATE-NC and α -synuclein, while APOE ε 4 was mainly associated with extracellular parenchymal and capillary A β pathology.

DISCUSSION: Although Alzheimer's disease pathology plays a central role in brain degeneration, coexisting pathologies can both exacerbate and independently contribute to it. These factors should be considered in patient stratification.

KEYWORDS

 α synuclein, amyloid β , apolipoprotein E ε 4, cerebral amyloid angiopathy, digital pathology, hippocampal degeneration, limbic-predominant age-related TDP-43 encephalopathy neuropathological changes, medial temporal lobe, mixed dementia, small vessels disease, tau

Highlights

- In aging individuals, amyloid β <u>peptide</u> (A β), tau pathology, limbic-predominant age-related TDP-43 encephalopathy neuropathological changes (LATE-NC), and amygdala-predominant α -synuclein pathology were interrelated but contributed independently to neurodegeneration.
- LATE-NC was the <u>strongest</u> driver of CA1 neuronal loss, while tau burden was the strongest predictor of global brain degeneration.
- Apolipoprotein E ε 4 was associated with both extracellular and capillary A β deposits, but not with tau burden.
- Temporal lobe small vessel disease was associated with both LATE-NC and amygdala-predominant α-synuclein pathology.
- Neural network models can reliably identify hippocampal pyramidal neurons on hematoxylin-stained histological slides.

1 | BACKGROUND

Amyloid β peptide (A β) and abnormal phosphorylated tau (pTau) protein aggregates are considered the most common pathological contributors to Alzheimer's disease (AD) in elderly patients. ¹⁻³ However, emerging evidence suggests that these hallmark AD neuropathological changes (ADNCs) may not fully account for the extent of neuronal loss observed in these individuals. A range of additional alterations, including other protein aggregates and vascular lesions, frequently coexists with ADNC and may contribute to brain degeneration through synergistic or additive mechanisms. ⁴⁻⁶

The medial temporal lobe (MTL) is particularly vulnerable to agerelated changes. It includes key structures such as the parahippocampal region, hippocampal formation, and amygdala, which are involved

in functions ranging from declarative memory formation to affective learning and familiarity signaling. The MTL is among the first regions affected by pTau aggregation and by atrophy associated with neurodegenerative dementia. It is also the first region where other pathological lesions accumulate, including specific variants of transactive response DNA-binding protein 43 (TDP-43) and α -synuclein (α Syn) pathologies. $^{9-13}$

TDP-43 aggregates that primarily accumulate in the MTL are classified as limbic-predominant age-related TDP-43 encephalopathy neuropathological changes (LATE-NC), a condition frequently observed alongside ADNC and distinct from other TDP-43 proteinopathies, such as amyotrophic lateral sclerosis or frontotemporal lobar degeneration. Similarly, while α Syn pathology in Lewy body disease typically follows a caudo-rostral progression (α Syn CR),

with early involvement of the brainstem, individuals with severe ADNC often exhibit an amygdala-predominant pattern (α Syn AmyP), in which α Syn aggregates accumulate earlier in the amygdala and other MTL structures than in the brainstem. 10,12 Although the role of $A\beta$ in promoting tau aggregation and spread has been recognized for years, ¹⁴ growing evidence suggests that pTau, TDP-43, and α Syn often colocalize within the same lesions and may interact to exacerbate pathology. 15-19

Hippocampal neuronal loss, particularly in the CA1 and subiculum subfields, has been associated with multiple brain pathologies. Strong evidence links degeneration in these regions to LATE-NC.9,11 Our recent observations indicate that α Syn AmyP is also associated with reduced neuronal density in CA1. 16 Additionally, ADNC, including pTau²⁰ and $A\beta$,²¹ as well as other lesions, have been implicated in hippocampal damage. These include argyrophilic grain disease (AGD),²² aging-related tau astrogliopathy (ARTAG),²³ granulovacuolar degeneration (GVD),²⁴ Hirano bodies,²⁵ and cerebrovascular factors like cerebral amyloid angiopathy (CAA),26 cerebral small vessel disease (SVD),²³ hippocampal calcification,²⁷ and atherosclerosis of the circle of Willis (AS).²⁸ However, given the frequent co-occurrence of these lesions, their individual contributions to neuronal loss remain uncertain.

Apolipoprotein E (APOE) is a major carrier of cholesterol and other lipids in the central nervous system.²⁹ The APOE ε 4 allele is one of the most extensively documented risk factors for AD30 and has been associated with numerous age-related neuropathological processes. 31-33 While there is strong evidence connecting the APOE $\varepsilon 4$ allele to the accumulation of extracellular A β deposits, ³⁴ its role in other neuropathological alterations remains less well understood.

This study aimed to investigate how age-related pathologies associated with AD contribute to brain degeneration, particularly in the hippocampus, while accounting for their interdependencies and determining the role of the APOE ε4 allele in this process. To achieve this, we trained a machine learning algorithm to detect pyramidal neurons, enabling a standardized quantification of neuronal density in the CA1 hippocampal subfield. We then applied linear regression analyses and structural equation modeling to examine the interactions among various MTL pathologies and assess their relative contributions to neuronal loss in CA1, overall brain weight, and cognitive impairment.

2 **METHODS**

2.1 Human autopsy cohort

This study included a total of 480 human autopsy cases from individuals aged \geq 50 years. The cases were part of the ARCK/LEUCALS (Alzheimer Research Center KU Leuven/Leuven Center for Amyotrophic Lateral Sclerosis) cohort. They were obtained from university or municipal hospitals in Leuven (Belgium; Ethics Committee Research [EC] UZ/KU Leuven identifiers: S52791, S55312, S59292, S64363); Brussels (Belgium; UCL-2020-355); Bonn, Offenbach am Main, and Ulm (Germany; EC UZ/KU Leuven identifier: S59295, Ulm identifier:

RESEARCH IN CONTEXT

- 1. Systematic review: Emerging experimental evidence indicates that interactions among amyloid β peptide (A β), tau, transactive response DNA-binding protein 43 (TDP-43), and α -synuclein aggregates may exacerbate neurodegeneration. However, the impact of these interactions remains largely unexamined in human cohorts.
- 2. Interpretation: Our findings suggest that neuronal loss and cognitive decline in elderly individuals result from both direct and synergistic effects of multiple coexisting pathologies. A β and amygdala-predominant α -synuclein appear to potentiate other lesions, while tau and TDP-43 are likely the main drivers of neurodegeneration. Additionally, arteriolosclerosis may serve as a mechanistic link between cerebrovascular damage and the accumulation of protein aggregates.
- 3. Future directions: Future research should prioritize identifying biomarkers that can detect co-pathologies accompanying $A\beta$ and tau. Stratifying patients based on these additional lesions may be essential to fully capture the heterogeneity of disease mechanisms, progression trajectories, and clinical symptoms in Alzheimer's disease.

58/08); as well as from GE Healthcare (UK; Clinical Trials.gov identifiers NCT01165554 and NCT02090855). Brain samples were collected in compliance with local and federal regulations governing the use of human tissue for research in Belgium, Germany, and the UK. All experiments were conducted after ethical clearance from the UZ/KU Leuven EC (identifier: \$65147).

To minimize potential confounders, we excluded cases with neuropathologically confirmed diagnoses of amyotrophic lateral sclerosis, frontotemporal lobar degeneration, Huntington's disease, multiple system atrophy, multiple sclerosis, brain tumors, encephalitis, severe hypoxic or hypoglycemic brain damage, or epilepsy-induced hippocampal sclerosis.

For 331 cases, the Global Clinical Dementia Rating (CDR) score³⁵ was retrospectively assigned based on standardized clinical examination reports from different clinicians, conducted 1 to 4 weeks before death. These reports included assessments of cognitive function and documented abilities such as self-care, dressing, eating habits, bladder and bowel continence, speech, writing, reading, memory problems, and spatial orientation. For 64 cases, Mini-Mental State Examination (MMSE)³⁶ scores were available and were converted to CDR scores using established cut-off values.³⁷

2.2 Gross examination

During the gross examination, brains were weighed, and brain slices were inspected for macroscopic hemorrhagic and ischemic infarcts. Additionally, the severity of AS plaques in the circle of Willis was graded using published criteria.³⁸ Values were excluded for this variable if fewer than 8 of the 12 circle of Willis arteries were assessed.

2.3 | Immunohistochemistry

After gross examination, either the left (n=434) or the right hemisphere (n=46) was formalin fixed. Tissue samples from various brain regions were used in this study, including the anterior MTL, the posterior MTL, the middle frontal gyrus, the occipital cortex, the midbrain, the pons, the medulla oblongata, the cerebellum, and the basal ganglia. The samples were then embedded in paraffin and sectioned into 5 μ m-thick slices for analysis.

The sections were stained using a panel of antibodies (see Table S1 in supporting information for the full list of stained regions, antibodies, and their concentrations). To prepare the sections, they were deparaffinized and subjected to epitope retrieval using citrate buffer (pH 6; Envision Flex Target Retrieval Solution, Dako, K8005) at 97°C for 10 minutes. For α Syn and A β staining, an additional step was included: a 5 minute incubation at room temperature in 98% to 100% formic acid. Tissue sections were incubated overnight with the primary antibody in a humid chamber at room temperature. The next day, either anti-mouse horseradish peroxidase (HRP)-linked secondary antibodies diluted in Tris-HCl-based diluent were applied for 30 minutes, or the VECTASTAIN ABC-HRP kit (Vector Laboratories) was used, involving a 30 minute incubation with the biotinylated secondary antibody followed by a 30 minute incubation with the ABC reagent at room temperature. The binding between the primary and secondary antibodies was visualized using a DAB solution applied for 10 minutes (Liquid DAB+ Substrate Chromogen System, Dako, catalog no. K3468). Finally, all slides were counterstained with hematoxylin using an autostainer, and coverslips were mounted automatically with a cover slipper (Leica Microsystems). Additionally, the autostainer was used to prepare hematoxylin-eosin (HE) sections for all slides.

2.4 Neuropathological assessment

Tissue examination and digital photography were conducted using a ZEISS Axio Imager 2 microscope with an Axiocam 506 camera and a DM2000 LED Leica microscope with a Leica DFC7000 T digital camera. Each case underwent a pathological assessment and diagnosis, with all parameters and their detailed operational definitions provided in Table S2 in supporting information and representative lesion images shown in Figure S1 in supporting information.

Phases of $A\beta$ plaque deposition, Braak stages for neurofibrillary tangles (NFTs) and Consortium to Establish a Registry for Alzheimer's Disease (CERAD) score for neuritic plaques (NPs) were obtained fol-

lowing established protocols. 2,3,39 The neuropathological diagnosis of ADNC was performed using the criteria published by the National Institute on Aging and Alzheimer's Association, with the ABC score applied as a general measure of ADNC severity. CAA severity was assessed according to Vonsattel grades and subtyped as type 1 (with capillary involvement) or type 2 (without capillary involvement). 40,41 Assessment of A β plaque and CAA pathology was based on immunostainings with an antibody detecting the A β_{17-24} epitope. Although this antibody can cross-react with the amyloid precursor protein (APP), it was recommended for detection of A β plaques and CAA because of its superior sensitivity for all types of A β plaques and the easy morphological distinction between APP expressing dystrophic neurites and neurons. 42,43

The presence of AGD and ARTAG in the MTL was assessed using AT8 staining.^{44,45} LATE-NC was diagnosed and staged based on recently published consensus guidelines.^{9,46} The presence of phosphorylated TDP-43 (pTDP-43) lesions in the dentate gyrus (DG) of the posterior hippocampus was also evaluated. Additionally, pTDP-43 staining was used to stage GVD progression according to established criteria.⁴⁷

The severity of α Syn pathology in the medulla oblongata, midbrain, amygdala, and temporal cortex was semi-quantitatively assessed and converted into a MTL-to-brainstem severity ratio, as described previously. ¹⁶ This ratio was used to distinguish between two spreading variants: α Syn AmyP (ratio > 1) and α Syn CR (ratio \leq 1).

The severity of SVD in the white matter of the inferior temporal and perirhinal cortex was semi-quantitatively scored on HE-stained sections from the posterior and anterior MTL, based on the number of affected vessels, as detailed earlier. ¹⁶ Microinfarctions and lacunar infarctions were identified on HE-stained sections as part of the diagnostic process. Using posterior MTL HE section we evaluated the presence of calcified vessels in the molecular layer of DG and CA1. Finally, we assessed the severity of Hirano body pathology in the CA1 region using categories based on lesion counts in three photographs taken at 200x magnification (623 \times 468 μ m each): 0 (no lesions), mild (1–8 lesions), moderate (9–25 lesions), and severe (\geq 26 lesions).

2.5 | APOE genotyping

Genomic DNA was extracted from either fresh-frozen or paraffinembedded brain tissue.

For 144 cases, genotyping of the *APOE* single nucleotide polymorphisms (SNPs) rs429358 and rs7412 was performed using low-coverage whole-genome sequencing, as previously described. ³³ Library preparation was conducted using the xGen cfDNA & FFPE DNA Library Preparation Kit (IDT) with barcoding, followed by equimolar pooling of the samples and sequencing with Avidity Chemistry (Arslan, 2023) at an average depth of 1x coverage on an AVITI instrument (Element Bioscience). Raw FASTQ files were aligned to the GRCh38 genome build using the Burrows–Wheeler Alignment tool and imputed using the Genotype Likelihoods IMputation and PHasing mEthod (GLIMPSE)⁴⁸ against the 1000 Genomes haplotype reference

panel. Allele dosages for both APOE SNPs were extracted to derive the APOE $\varepsilon 2$, $\varepsilon 3$, and $\varepsilon 4$ alleles. All SNPs had genotype probability > 0.9.

For 18 samples, APOE genotyping was performed using Sanger sequencing. DNA was amplified using simplex polymerase chain reaction (PCR; forward primer: GCCTACAAATCGGAACTGGA, reverse primer: CTCGAACCAGCTCTTGAGGC) with Platinum Taq (Thermo Fisher Scientific). After purification of the PCR products with Illustra ExoProStar (Cytiva), dideoxy chain termination was conducted with the BigDye Terminator v3.1 Cycle Sequencing Kit (Thermo Fisher Scientific). Sequencing was carried out on an ABI 3730XL DNA Analyzer (Thermo Fisher Scientific) according to the manufacturer's protocol. Sequence analysis was performed using novoSNP v3.9.1 and SnapGene v6.03 software (GSL Biotech LLC).

Additional APOE genotyping data were available for 120 cases, obtained using PCR followed by *Hhal* restriction enzyme digestion, as previously described.⁴⁹ For another 85 cases, APOE genotype information was provided by GE Healthcare in the context of clinical trials NCT01165554 and NCT02090855.

2.6 Automated neuronal detection algorithm

2.6.1 | Input dataset

Pyramidal neurons in the CA1 subfield of the posterior hippocampus were manually annotated using the annotation tool in QuPath (v0.5.1) across 801 images derived from pTDP-43 $^{\rm Ser409/Ser410}$ -stained sections of 267 individuals, in accordance with the criteria described by Gawor et al. $^{\rm 16}$ In short, three consecutive 500 \times 500 μm images were taken from the posterior CA1 sector, covering most of the CA1 length. Images were selected to avoid the inclusion of artifacts and larger blood vessels.

In addition to neuronal annotation, non-neuronal structures, such as blood vessels, were annotated in 72 pTDP-43-stained images of the CA1 region and 16 images from the molecular layer of the DG and CA1. Each image covered an area of $500 \times 500 \ \mu m$ and was captured using a ZEISS Axio Imager 2 Microscope equipped with an Axiocam 506 camera, a 20x objective, and auto-exposure settings. The dataset encompassed a range of conditions, including varying levels of neuronal loss, differences in fixation times, durations of paraffin embedding, *post mortem* intervals (PMIs), and phases of photobleaching.

2.6.2 | Object detection

The following image-processing pipeline consists of a collection of inhouse Python (version 3.10) scripts, in which object detection and neuron classification are integrated into a unified framework that enables large-scale execution without the need for manual intervention. A schematic illustrating the workflow of the complete neuronal detection algorithm is shown in Figure S2 in supporting information (https://github.com/neuropathology-lab/neurodetection).

Image-object detection algorithms typically expect objects of interest to appear bright against a dark background. Because the opposite is true for H&E staining, where cells appear dark against a lighter background, the images were first inverted. A mild Gaussian blur (using scikit-image's Gaussian filter, version 0.24.0) was applied to mitigate potential noise introduced during image acquisition. To restrict downstream processing to relevant regions, the foreground was segmented from the background by thresholding. Because this approach relies on intensity differences rather than color information, images were first converted to grayscale to reduce complexity and improve robustness.

then performed using Thresholding was the age.filters.threshold_local function on a subsampled version of the image to reduce the influence of potential artifacts. The foreground (i.e., pixels exceeding the threshold) was subsequently scanned for local maxima using skimage.feature.peak_local_max, which identifies regions that are brighter than their immediate surroundings. Because this method can detect redundant peaks, the DBSCAN algorithm from scikit-learn (version 1.5.2) was applied to spatially cluster nearby local maxima that likely belong to the same object. This offers two key advantages: it reduces the number of image slices passed to the model, thereby improving computational efficiency; and it prevents objects containing multiple local maxima from being counted as separate instances. In practice, points that were clustered together by DBSCAN were merged into a single point, of which the center was calculated as the midpoint of all local maxima belonging to the cluster.

2.6.3 | Creation of classifier training data

Extracting objects for the creation of the training data was slightly adapted from the protocol described above. For this purpose, a wider net was cast in detecting objects to generate enough negative controls for training. Specifically, the above protocol was cut short after thresholding the foreground from the background. Small holes in the thresholded image were then filled using scipy.ndimage.binary fill holes (version 1.15.2) to generate rounded objects, as is expected when segmenting cells. Each connected streak of foreground-assigned pixels was then labeled as a standalone object and assigned a unique label using the skimage.measure.label function. The manually annotated "positive" neuron dataset was created by extracting a 100 × 100 pixel bounding box around the center of each annotation. Then, for each manual annotation, that center coordinate was matched to its corresponding object in the thresholded image. All pixels belonging to the matching object were set to zero, resulting in a neuron-free foreground.

The negative dataset was then created by randomly sampling the remaining objects, which did not contain any neurons. This method was chosen over simply selecting random regions, as it ensures that the "negative" part of the training dataset contains realistic objects that could potentially be picked up by the object detection algorithm described above.

A total of 122,801 single-object images were extracted, with 31,273 annotated as "Positive" and 91,528 as "Negative." These were split into

training (60%), validation (20%), and test (20%) subsets. All training images were saved as 32-bit depth RGB png files.

2.6.4 | Training of image classifier

A binary classifier was trained using transfer learning with ResNet-34 as the base architecture to distinguish photos of neurons from non-neurons. ResNet-34, a pre-trained convolutional neural network trained on ImageNet, was fine-tuned for this task. Model training was performed using PyTorch via FastAl v2. Training was conducted over three epochs using the vision_learner and fine_tune functions. During the first epoch, only the final layer was trained while the remaining layers were frozen. In the subsequent epochs, all layers were unfrozen and trained. A default batch size of 64 and a base learning rate of 0.002 were used. The validation error rate was 10.8% after the first epoch, decreasing to 5.5% by the third epoch, after which it plateaued. Each training round took \approx 30 minutes on a local CPU with six cores and 16 GB of RAM.

2.6.5 | Estimating neuronal density

Three images of the posterior CA1 region were collected from each of the 480 cases included in this study, following the same guidelines as those used for the input dataset. Object detection was performed, and the identified objects were classified as either neurons or nonneurons using the trained classifier. Objects within 10 μm of the image edge were excluded. If two detected neurons were within 15 μm of each other, one was randomly removed to prevent duplicate counting. Finally, neuron density was calculated for each case in neurons per mm^2 .

2.6.6 | Validation on independent dataset

Additionally, 60 randomly selected photos, not included in the training dataset, were manually annotated by an independent rater who was not involved in the training annotation process. The number of neurons identified by the automated neuronal detection algorithm in each photo was compared and correlated with the counts identified by the human rater.

2.7 | Statistical analysis

Statistical analyses were conducted in RStudio (version 2024.09.0) using R 4.3.0. Differences in brain degeneration across pathology combinations were assessed using Kruskal–Wallis tests, followed by pairwise Wilcoxon rank-sum tests with Bonferroni–Holm (BH) correction. Spearman correlation was used to examine the relationships between demographic variables (age at death and sex) and neuropathological parameters. Additionally, semi-partial Spearman correlation, control-

ling for age at death, was performed to assess associations between each pair of neuropathological parameters. All correlation *P* values were adjusted using the BH method. Furthermore, three series of linear regression analyses were conducted to examine the relationships between brain degeneration measures (including CA1 neuronal density, brain weight, and CDR) and neuropathological parameters, each incorporating a different set of covariates. All variables were standardized, and *P* values for neuropathological parameters were BH-adjusted within each regression series.

Additionally, structural equation model analyses were performed using the lavaan package (version 0.6.16). The directionality of arrows in models was decided based on the literature on protein aggregate interactions (Table S3 in supporting information), however, the path $\alpha \text{Syn} \rightarrow \text{LATE}$ had to be reversed to avoid non-recursive models. Model parameters were estimated using maximum likelihood estimation with robust standard errors, a Satorra–Bentler scaled test statistic, and the NLMINB optimization method. Model fit was assessed using the robust comparative fit index (CFI; good fit > 0.97), robust standardized root mean squared residual (SRMR; good fit < 0.05), and standardized root mean square error of approximation (RMSEA; good fit < 0.05).

3 RESULTS

The study cohort included 480 individuals aged 50 to 99 years, with 52.1% being male and 50.6% were classified as cognitively impaired (CDR > 0, assessed in 395 cases). A detailed summary of demographics, neuropathological parameters, and the number of cases analyzed is provided in Table 1. The operationalization of the parameters is detailed in Table S2.

3.1 Neuronal detection algorithm

To assess the density of pyramidal neurons in the posterior CA1 subfield of the hippocampus across all cases, a pyramidal neuron detection algorithm using a neural network classifier was trained (Figure 1A). Examples of neuron detections are shown in Figure 1B and Figure S3 in supporting information. Classifier metrics for the validation dataset were as follows: accuracy: 94.4%, sensitivity: 88.4%, specificity: 96.5%, precision: 90%. Similar metrics were also obtained on the test dataset. For 60 randomly selected images, independently evaluated by a reviewer not involved in classifier training, the Spearman correlation coefficient between the algorithm's output and the human ratings was 0.83 (Figure S4 in supporting information), indicating high reliability of the detection algorithm.

The mean neuronal density in the CA1 subfield in our sample was 163.3 neurons per $\rm mm^2$ (standard deviation [SD] = 67.4), with values ranging from 1.3 to 387.5. Figure $\rm 1C$ illustrates the distribution of neuronal damage in cognitively intact and cognitively impaired individuals. The distribution of brain weights, stratified by cognitive status, is presented in Figure S5 in supporting information.

TABLE 1 Summary statistics of cohort demographics and neuropathological parameters.

Parameter	Mean (SD)	Frequency (%)	Min-max	n
Age at death (y)	74.6 (10.8)	-	50-99	480
Sex (male)	-	52.1%	-	480
CDR	1.06 (1.26)	-	0-3	395
Cognitively intact (CDR $= 0$)	-	49.4%	-	-
MCI (CDR = 0.5)	-	6.3%	-	-
Dementia (CDR > 0.5)	-	44.3%	-	-
Neuronal density CA1 (per mm²)	163.3 (67.4)	-	1.3-387.5	480
Brain weight (g)	1238.5 (171.6)	-	585-1700	333
PMI (hours)	35.2 (30.5)	-	1.5-144	423
APOE	-	-	-	367
ε2/ε2	-	0.8%	-	-
ε2/ε3	-	10.1%	-	-
ε2/ε4	-	2.2%	-	-
ε3/ε3	-	55%	-	-
ε3/ε4	-	27%	-	-
ε4/ε 4	-	4.9%	-	-
Braak NFT stages (pTau)	2.7 (1.9)	-	0-6	480
$A\beta$ phases	2.6 (2)	-	0-5	480
CERAD score (NPs)	0.9 (1.2)	-	0-3	480
LATE-NC stages	0.5 (0.9)	-	0-3	480
pTDP-43 DG	-	10.2%	0-1	479
αSyn variant	-	-	-	480
No αSyn	-	67.30%	-	-
Amygdala-predominant	-	10.6%	-	-
Caudo-rostral	-	22.1%	-	_
SVD in temporal cortex	0.9 (0.9)	-	0-3	366
AS severity	1.6 (0.8)	-	0-3	298
CAA type	-	-	-	480
No CAA	-	44.0%	-	-
Type 1	-	30.0%	-	-
Type 2	-	26.0%	-	-
CAA severity	1(1)	-	0-3	480
Hippocampal calcifications	-	23.5%	0-1	442
Infarctions	-	18.4%	0-1	418
ARTAG	-	19.4%	0-1	324
AGD	-	12.6%	0-1	445
Hirano bodies severity	1 (0.7)	-	0-3	278
GVD stages	1.4 (1.7)	-	0-5	355

Note: Continuous and ordinal variables are presented as mean and SD. Binary and categorical variables are reported as the percentage of cases exhibiting the specified characteristics.

Abbreviations: $A\beta$ phases, phases of amyloid β plaque pathology; AGD, argyrophilic grain disease; α Syn, α synuclein pathology; APOE, apolipoprotein E gene; ARTAG, aging-related tau astrogliopathy; AS, atherosclerosis of the circle of Willis; CAA, cerebral amyloid angiopathy; CDR, Clinical Dementia Rating; CERAD, Consortium to Establish a Registry for Alzheimer's Disease; GVD, granulovacuolar degeneration; LATE-NC, limbic-predominant age-related TDP-43 encephalopathy neuropathological change; MCI, mild cognitive impairment; NFT, neurofibrillary tangle; NP, neuritic plaque; PMI, post mortem interval; pTau, phosphorylated tau; pTDP-43 DG, phosphorylated TDP-43 in the dentate gyrus; SD, standard deviation; SVD, small vessel disease.

15525279, 2025, 7, Downloaded from https

(A)

Post-mortem human brains

Neuropathological examination

Manual neuron

annotation CA1

Brain weight

Cognitive dementia rating

Genotyping

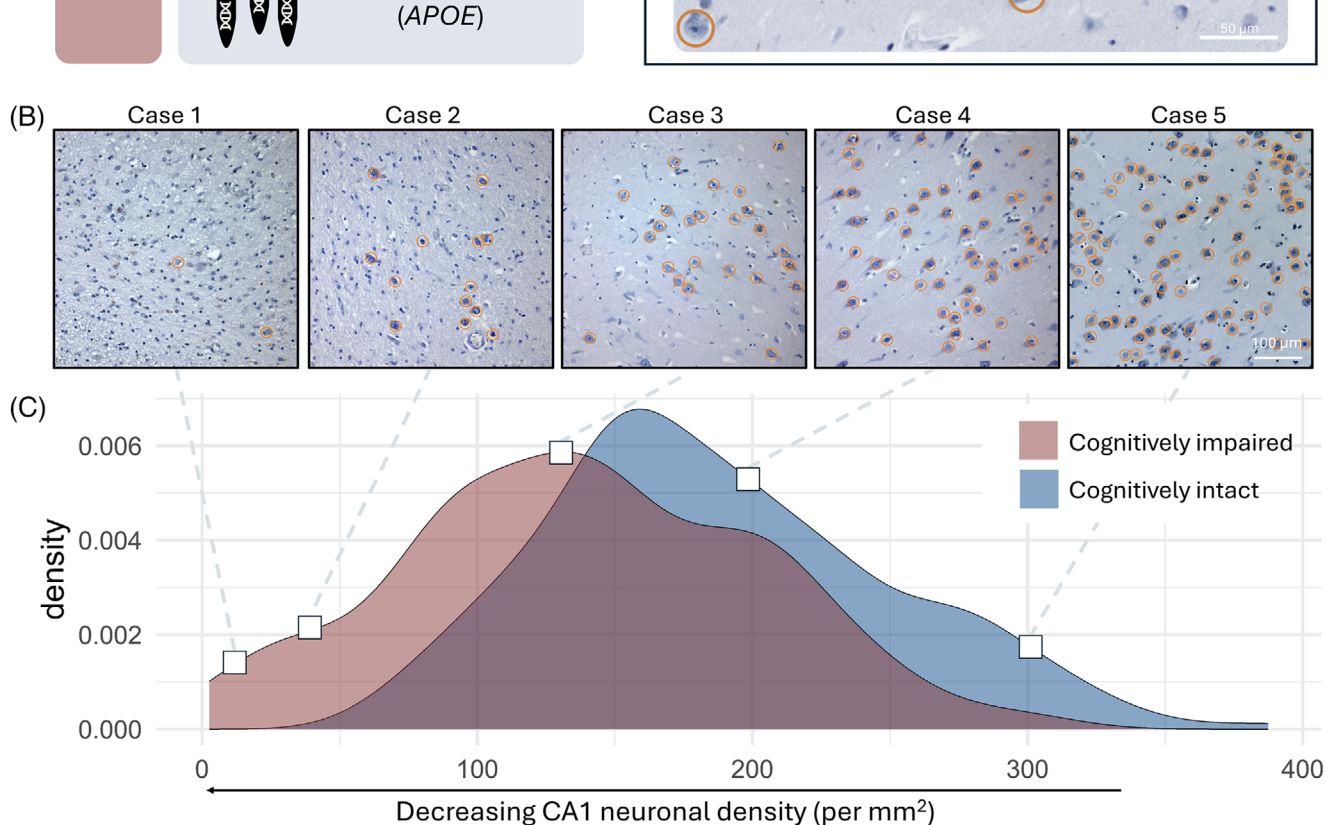


FIGURE 1 A, Schematic representation of the study design. B, Representative images from the CA1 subfield of the posterior hippocampus in five different cases, with neurons identified by the trained classifier marked by orange circles. C, Density plot showing the distribution of CA1 neuronal densities in cognitively impaired (CDR > 0, n = 195) and cognitively intact (CDR = 0, n = 200) cases. Cognitive impairment status was unavailable for 85 cases. APOE, apolipoprotein E gene; CDR, Clinical Dementia Rating score.

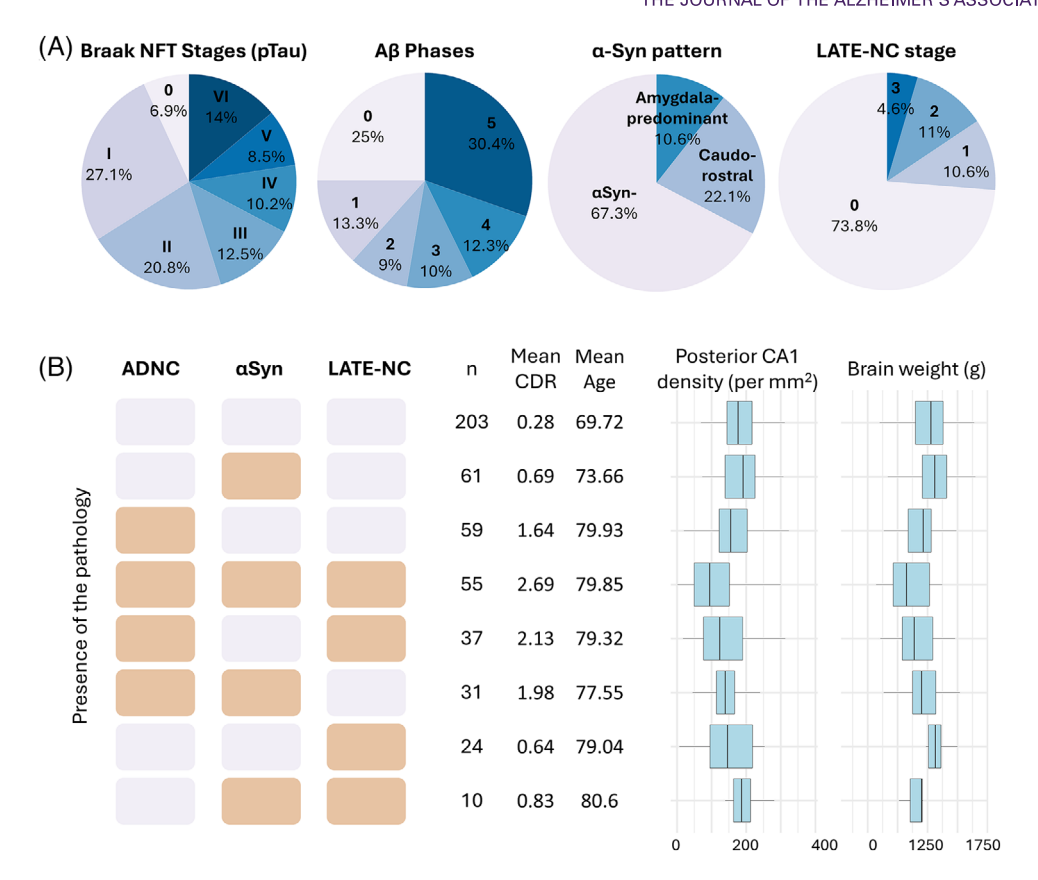


FIGURE 2 Combinations of neuropathological lesions and their brain degeneration correlates. A, Proportion of cases with specific pathological lesions identified in this study in total sample of 480 cases. B, Overview of combinations of moderate or severe ADNC, α Syn pathology, and LATE-NC in the study cohort, arranged in descending order of prevalence (left panel). The number of cases in each group, their mean CDR score, and mean age at death are reported (middle panel). Boxplots illustrate neuronal density in the CA1 and brain weight for each combination (right panel). Horizontal bold lines in the boxplots represent median values, box margins indicate the 25th and 75th percentiles, and whiskers display the full range of observed values. A summary of the Kruskal-Wallis analysis with pairwise Wilcoxon tests comparing brain degeneration measures across different combinations can be found in Table S5 in supporting information. A β phases, phases amyloid β plaque deposition; ADNC, Alzheimer's disease neuropathologic changes; aSyn, a-synuclein pathology; CDR, Clinical Dementia Rating score; LATE-NC, stages of limbic-predominant age-related TDP-43 encephalopathy neuropathological changes; NFT, neurofibrillary tangle; pTau, phosphorylated tau pathology.

Prevalence of mixed pathologies

The sample encompassed a broad range of ADNC and LATE-NC severities, as well as two α Syn pathology variants (Figure 2A). Within the cohort, 93.1% of cases exhibited pTau aggregates, 75% had Aβ deposits, 32.7% displayed α Syn pathology, and 26.3% had LATE-NC.

Mixed pathologies were common (Figure 2B, Table \$4 in supporting information). Among the 182 cases with moderate to severe ADNC, 92 (51%) also had LATE-NC. Additionally, 86 (47%) exhibited αSyn pathology, including 45 with the AmyP variant and 41 with the CR variant. A triple pathological combination—comprising ADNC, α Syn, and LATE-NC-was observed in 55 cases, accounting for 30% of all cases with moderate to severe ADNC.

Individuals with triple pathology had the lowest neuronal density in the CA1 region (mean = 108.1), significantly lower than individuals with ADNC only (mean = 160.9, P value < 0.001) or those without any of the three pathologies (mean = 182.2, P value < 0.001), as confirmed

by a Kruskal-Wallis test followed by pairwise Wilcoxon comparisons with BH correction (Table \$5 in supporting information). Additionally, individuals with triple pathology showed the greatest cognitive impairment at death across all pathology combinations (all BH-corrected P value < 0.05).

Correlations among age-related neuropathologies, age at death, and sex

We analyzed relationships among key age-related neuropathological markers, age at death, and sex using Spearman correlation (Table S6 in supporting information). The neuropathological parameters included A β , pTau, NPs, LATE-NC stages, TDP-43 positivity in the DG, α Syn variants, temporal lobe SVD, AS, CAA severity, CAA type 1, hippocampal vascular calcification, multiple old brain infarctions, ARTAG, AGD, Hirano bodies, and GVD.

15525279, 2025, 7, Downloaded

on [15/10/2025]. See the

of use; OA articles

are governed by the applicable Creative Comm

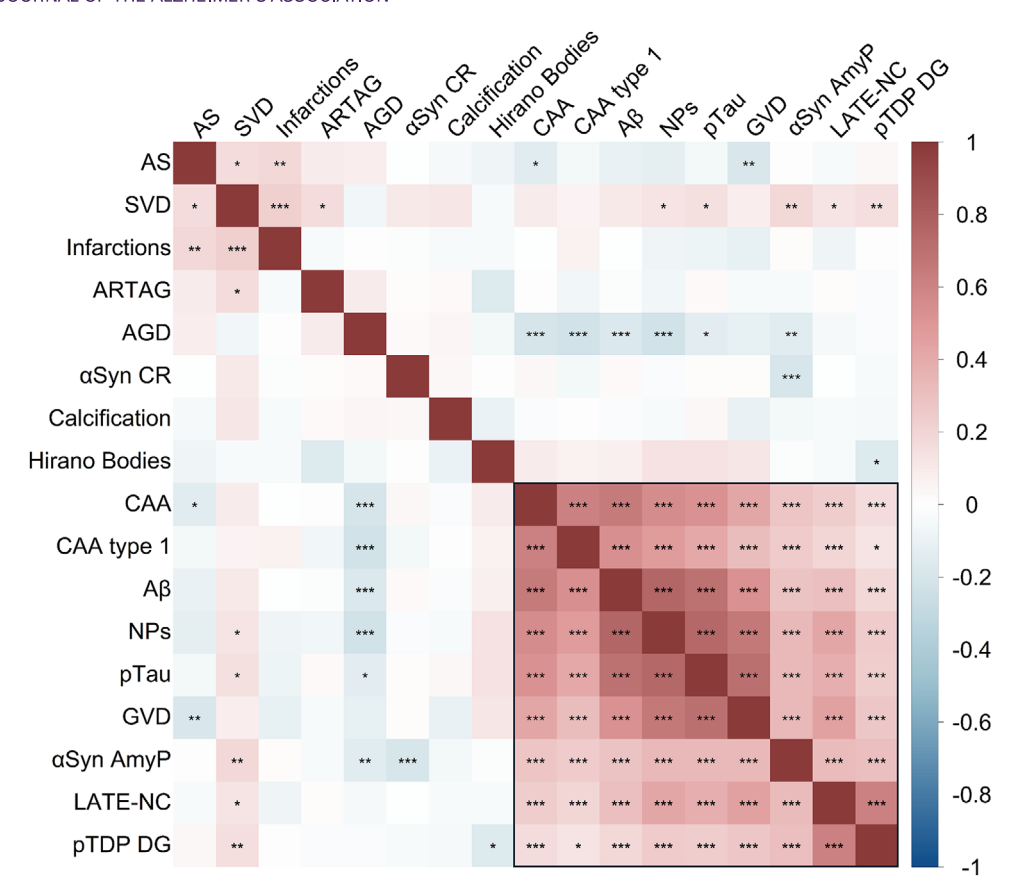


FIGURE 3 Heatmap displaying the results of a semi-partial Spearman correlation of neuropathological lesions, corrected for age at death. Stars indicate significance levels of P values adjusted using the Bonferroni-Holm correction (*P value < 0.05, **P value < 0.01, ***P value < 0.01). The shade of each tile represents the strength and direction of the correlation. The order of tiles has been arranged using hierarchical clustering with complete linkage. A square highlights the spectrum of Alzheimer's disease-related lesions that are strongly intercorrelated. $A\beta$, represents the phase of amyloid β plaque deposition in the brain; AmyP, amygdala-predominant pattern; AGD, argyrophilic grain disease; α Syn, α -synuclein pathology; ARTAG, aging-related tau astrogliopathy; AS, severity of atherosclerosis of the circle of Willis; CAA, severity of cerebral amyloid angiopathy; CAA type 1, type 1 of cerebral amyloid angiopathy; CR, caudo-rostral pattern; GVD, stage of granulovacuolar degeneration; LATE-NC, stages of limbic-predominant age-related TDP-43 encephalopathy neuropathological changes; Hirano bodies, severity of Hirano body pathology; NP, CERAD neuritic plaque score; pTau, represents the Braak NFT stage of phosphorylated tau pathology; pTDP-43 DG, phosphorylated TDP-43 in the dentate gyrus; SVD, small vessel disease score.

A positive correlation with age at death was observed for the majority of neuropathological parameters, except for α Syn CR (P value = 0.145), hippocampal calcification (P value = 0.897), Hirano bodies (P value = 0.669), and AGD (P value = 0.08). Regarding sex differences, the only significant finding was a greater prevalence of α Syn CR in males (P value = 0.012). Additionally, trends approaching significance (P value < 0.1) were observed for associations between females and increased pTau and GVD, as well as males and a higher prevalence of infarctions.

Next, we investigated associations between individual lesions using Spearman correlation analysis, adjusted for age (Figure 3). Correlation coefficients, exact P values, and the number of pairwise cases are provided in Table S7 in supporting information. The analysis revealed strong correlations among ADNC, CAA, GVD, αSyn AmyP, and LATE-NC parameters (BH-corrected P values < 0.05 for all correlation pairs). Additionally, temporal SVD correlated with ADNC, LATE-NC, α Syn AmyP, and ARTAG. Cerebrovascular parameters such as SVD,

AS, and multiple old infarctions were correlated with one another. AGD showed a negative correlation with ADNC, CAA, and α Syn AmyP pathology.

3.4 Role of brain pathologies in hippocampal and global brain degeneration

To assess the impact of neuropathological lesions on brain degeneration, we conducted three sets of multiple linear regression analyses. Neuropathological lesions served as independent variables, while brain degeneration was estimated using three dependent variables: posterior CA1 neuronal density (reflecting MTL damage), brain weight (indicating overall atrophy), and CDR score (serving as a marker of cognitive impairment).

The first series of analyses was adjusted for age at death, sex, and cohort. The second series was additionally controlled for overall ADNC

THE JOURNAL OF THE ALZHEIMER'S ASSOCIATION

levels. In the third series, we further adjusted for the PMI; this analysis was restricted to non-ADNC variables that remained significant in the second set. Complete statistical results, including standardized regression coefficients and sample sizes, are available in Tables S8–S10 in supporting information and summarized in Figures S6–S7 in supporting information.

All ADNC parameters (pTau, $A\beta$, and NPs) were associated with all brain degeneration measures (Figure 4A, Series 1; P value < 0.001 for all), emphasizing the need to control for these factors when analyzing the role of other neuropathologies.

After adjusting for ADNC (Figure 4B, Series 2), both LATE-NC stages and TDP-43 inclusions in the DG were negatively associated with CA1 neuronal density ($\beta = -0.26$, P value < 0.001; $\beta = -0.32$, P value < 0.001) and associated with increased cognitive impairment ($\beta = 0.16$, P value < 0.001 for both). α Syn AmyP pathology was linked to CA1 degeneration ($\beta = -0.16$, P value < 0.001) and cognitive impairment ($\beta = 0.09$, P value = 0.03). The α Syn CR variant was also associated with cognitive impairment ($\beta = 0.09$, P value = 0.04).

Moreover, vascular parameters such as SVD in the temporal cortex and AS severity were associated with CA1 neuronal loss ($\beta=-0.13$, P value = 0.02; $\beta=-0.15$, P value = 0.01). AS severity was also associated with greater cognitive impairment ($\beta=0.16$, P value = 0.001). CAA severity was positively associated with cognitive impairment ($\beta=0.10$, P value = 0.049), while CAA type 1 was correlated with increased brain weight ($\beta=0.14$, P value = 0.03). GVD stages were related to cognitive impairment ($\beta=0.21$, P value < 0.001). Interestingly, Hirano bodies were linked to increased CA1 neuronal density ($\beta=0.11$, P value = 0.049). Other parameters, including hippocampal vascular calcifications, multiple old infarctions, ARTAG, and AGD, showed no association with brain degeneration measures in models with or without ADNC adjustment.

Models showing significant associations between pathological factors and brain degeneration measures after adjusting for ADNC were further controlled for PMI (Series 3), which resulted in a reduced sample size. After including this covariate, the associations between SVD and CA1 neuronal density ($\beta = -0.1$, P value = 0.052) and between α Syn CR and cognitive impairment ($\beta = 0.07$, P value = 0.057) were no longer statistically significant but remained at a trend level. All other associations remained significant.

3.5 | Modeling connections between AD-related lesions

Structural equation models examined the interactions among neuropathological parameters, their association with the APOE $\varepsilon 4$ gene dose, and their effects on brain degeneration measures. Each model demonstrated a good fit based on standard criteria (Table S11 in supporting information). Detailed summary statistics are available in Tables S12–S17 in supporting information. All reported path estimates are standardized (expressed in SD units) to enable direct comparison of effect sizes across paths.

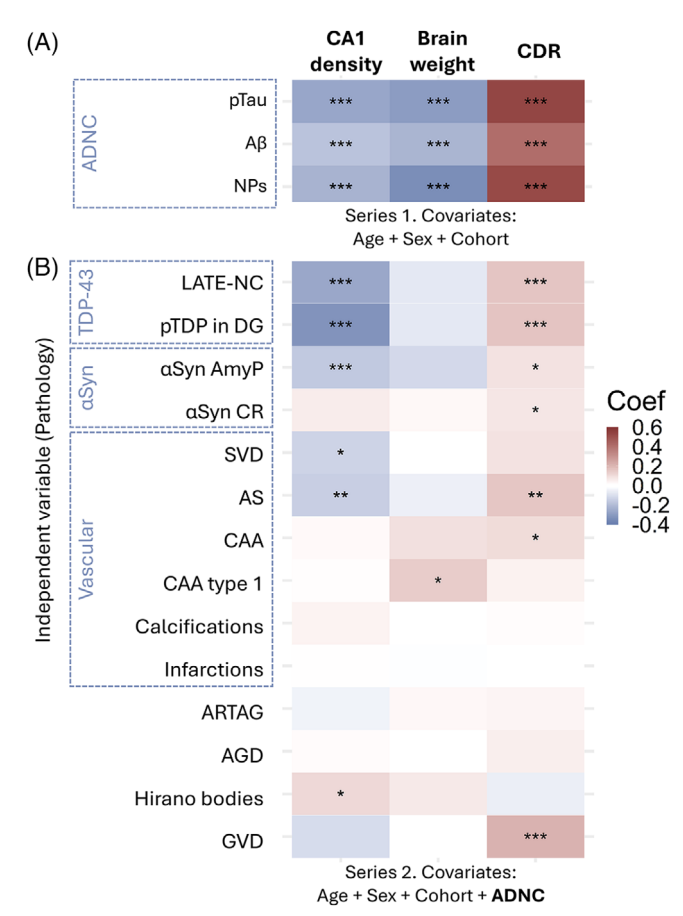


FIGURE 4 Heatmap showing standardized coefficients from multiple linear regression analyses evaluating brain degeneration measures as dependent variables and neuropathological lesions as independent variables. Regression models were adjusted for age at death, sex, and cohort (A, Series 1) and for the overall severity of Alzheimer's disease neuropathological changes (B, Series 2). The colors of the tiles represent the direction and strength of the coefficients for each neuropathological lesion. Asterisks indicate P values after Bonferroni-Holm correction within each panel (* P value < 0.05, ** P value < 0.01, *** P value < 0.001). A β , represents the phase of amyloid β plaque distribution in the brain; AGD, argyrophilic grain disease; α Syn, α synuclein pathology; AmyP, amygdala-predominant pattern; ARTAG, aging-related tau astrogliopathy; AS, severity of atherosclerosis of the circle of Willis; CAA, severity of cerebral amyloid angiopathy; CAA type 1, type 1 of cerebral amyloid angiopathy; CDR, Clinical Dementia Rating score; CR, caudo-rostral pattern; GVD, stage of granulovacuolar degeneration; LATE-NC, stage of limbic-predominant age-related TDP-43 encephalopathy neuropathological changes; Hirano bodies, severity of Hirano body pathology; NP, CERAD score for neuritic plaque pathology; pTau, phosphorylated tau; pTDP-43 DG, phosphorylated TDP-43 in the dentate gyrus; SVD, small vessel disease score.

Interrelations among core parameters were observed (Model 1, Figure 5, n=480), with the most robust associations found between A β and CAA severity (estimate = 0.67, P value < 0.001) and A β and pTau (estimate = 0.52, P value < 0.001), followed by LATE-NC and A β

15525279, 2025, 7, Downloaded from

Luther University Halle-Wittenberg, Wiley Online Library on [15/10/2025]. See the

of use; OA articles

are governed by the applicable Creative Comm

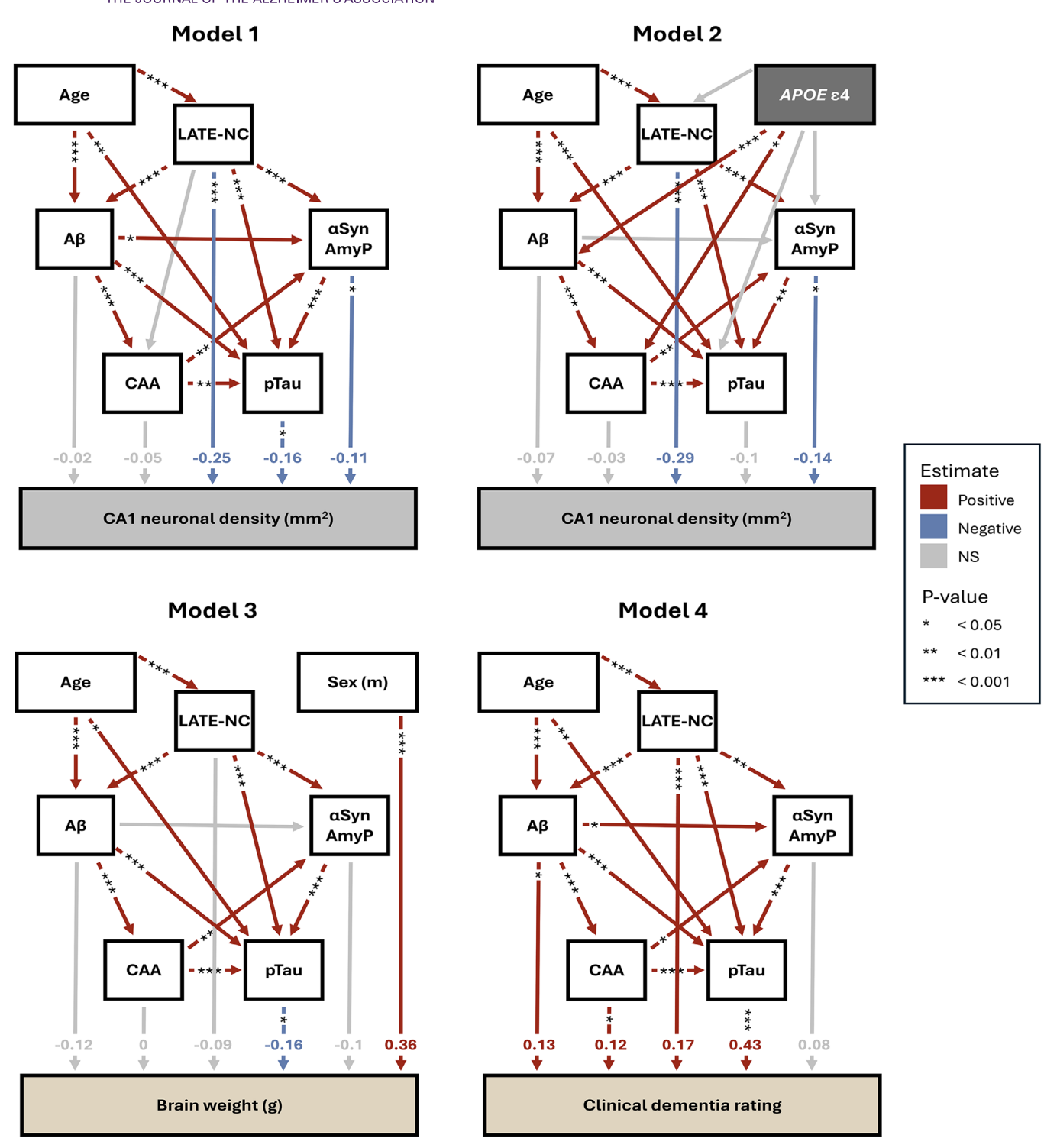


FIGURE 5 Structural equation models were used to investigate the relationships between neuropathological lesions associated with the AD spectrum and measures of brain degeneration. Model 1 (n = 480) examined the associations between AD-related lesions and neuronal density in the posterior CA1 region. The association between LATE-NC and CAA was not significant and was excluded from subsequent models. Model 2 (n = 367) explored the effect of the $APOE \, \varepsilon 4$ gene dose on the accumulation of neuropathological lesions. A complementary model incorporating CAA type 1 is presented in Figure S8 in supporting information. Additionally, we analyzed the association between brain lesions and total brain weight in Model 3 (n = 333) and between neuropathological lesions and global cognitive impairment, as measured by the CDR, in Model 4 (n = 397). All directional relationships included in the models are represented by arrows. The color of each arrow indicates the sign of the estimate, except for non-significant (NS) path estimates (P value ≥ 0.5), which are shown in gray. Standardized estimates for paths involving brain degeneration parameters are indicated at the tip of each arrow. A β , reprensents the phase of amyloid β plaque deposition; AD, Alzheimer's disease; α Syn, α Synuclein pathology; AmyP, amygdala predominant pattern; α POE, apolipoprotein E gene; CAA, severity of cerebral amyloid angiopathy; CDR, Clinical Dementia Rating score; LATE-NC, stages of limbic-predominant age-related TDP-43 encephalopathy neuropathological changes; pTau, represents the Braak NFT stage for the distribution of phosphorylated tau.

(estimate = 0.29, P value < 0.001) and LATE-NC and α Svn AmvP (estimate = 0.27, P value < 0.001). Additional associations were observed between LATE-NC and pTau (estimate = 0.15, P value < 0.001), α Syn AmyP and CAA (estimate = 0.15, P value = 0.002), pTau and α Syn AmyP (estimate = 0.11, P value < 0.001), pTau and CAA (estimate = 0.13, P value = 0.001), and between α Syn AmyP and A β (estimate = 0.11, P value = 0.034). No association was found between LATE-NC and CAA (estimate = 0.05, P value = 0.174). Subsequent models were developed based on the significant associations among neuropathological parameters identified in Model 1.

After accounting for interrelationships among neuropathological parameters, Model 1 (Figure 5) also assessed their direct associations with CA1 neuronal density. LATE-NC (estimate = -0.26, P value < 0.001), pTau (Estimate = -0.16, P value = 0.014), and α Syn AmyP (estimate = -0.11, P value = 0.027) were associated with reduced CA1 neuronal density, whereas A β (estimate = -0.02, P value = 0.81) and CAA severity (estimate = -0.05, P value = 0.394) showed no effect. Additionally, a supplementary model was developed to assess whether SVD in the temporal lobe directly influences CA1 neuronal density (Model S1, Figure S8 in supporting information, n = 366). The results showed a non-significant direct association between SVD and CA1 neuronal loss (estimate = -0.06, P value = 0.237). However, SVD was associated with both LATE-NC (estimate = 0.14, P value = 0.013) and α Syn AmyP (estimate = 0.11, P value = 0.023).

Including the APOE ε4 gene dose in the model (Model 2, Figure 5; n = 367) revealed a significant association with A β pathology (estimate = 0.3, P < 0.001) and CAA severity (estimate = 0.11, P = 0.006). While the association between APOE ε4 and LATE-NC did not reach statistical significance, it approached the threshold (estimate = 0.11. P = 0.057). In contrast, no significant associations were found between APOE ε 4 and pTau (estimate = 0.03, P = 0.401) or α Syn AmyP (estimate = 0.08, P = 0.199). When CAA severity was replaced with the presence of CAA Type 1 (Model S2, Figure S6; n = 367), a direct association with APOE ε 4 was also observed (estimate = 0.29, P < 0.001).

Next, we examined the pathological lesions associated with decreased brain weight (Model 3, Figure 5, n = 333). To account for a potential confounder, we included a path between brain weight and sex in this model. pTau was the only pathology with a direct effect that reached significance level (estimate = -0.16, P value = 0.047). Although α Syn AmyP (estimate = -0.10, P value = 0.071), LATE-NC (estimate = -0.09, P value = 0.12), and A β (estimate = -0.12, P value = 0.184) also had negative estimates for the path to brain weight, they did not reach statistical significance.

Finally, a model examining neuropathological pathways influencing cognitive impairment (Model 4, Figure 5, n = 395) identified a strong effect of pTau (estimate = 0.43, P value < 0.001). Nevertheless, other pathologies also contributed to an increased likelihood of cognitive impairment, including LATE-NC (estimate = 0.17, P value < 0.001), $A\beta$ (estimate = 0.13, P value = 0.04), and CAA severity (estimate = 0.12, P value = 0.028). The association between α Syn AmyP and cognitive impairment was borderline significant (estimate = 0.08. P value = 0.051).

DISCUSSION

Our findings highlight that neurodegeneration in age-related dementias results from the complex interaction of multiple pathologies. We found that A β , pTau, LATE-NC, and amygdala-predominant α Syn contributed to brain degeneration both independently and through their synergistic effects. While pTau was the primary driver of global brain atrophy, neuronal loss in the CA1 subfield of the posterior hippocampus was predominantly, though not exclusively, associated with LATE-NC. Additionally, we identified an association between SVD in the temporal white matter and amygdala-predominant α Syn pathology, and highlighted its link with LATE-NC. Furthermore, our analysis showed that the APOE ε4 allele is associated with increased extracellular and capillary $A\beta$ deposition but is not directly influenced by pTau burden or amygdala-predominant α Syn.

Consistent with previous studies, 4-6 we found that mixed pathologies are highly prevalent in the brains of older adults. Only 32% of individuals with moderate to severe AD pathology had neither LATE-NC nor α Syn co-pathology. Individuals with AD and both copathologies showed significantly greater cognitive impairment than other patient groups, supporting previous findings that those with "quadruple" lesions experience a more aggressive decline in cognitive function. 50 Although pTau showed the strongest direct association with global cognitive decline, A β , CAA, and LATE-NC each contributed independent effects as well.

We observed that neuronal loss in CA1 subfield of hippocampus among older adults did not follow a binary pattern of intact tissue versus complete loss, that is, hippocampal sclerosis, but instead occurred along a continuum. LATE-NC emerged as the strongest predictor of hippocampal damage, consistent with prior studies. 11,51-53 However, tau also showed an independent effect in the full-cohort model, supporting findings from imaging studies that both pathologies contribute to MTL degeneration.⁵⁴ Additionally, α Syn showed an independent association with CA1 degeneration—an effect we previously suspected but were unable to confirm in our smaller cohort.¹⁶

Using structural equation modeling, we found that the investigated proteinopathies were reciprocally related, consistent with evidence from cellular, animal, and in vivo studies suggesting that protein aggregates may promote misfolding and accumulation across pathologies. 14,15,17-19 The strongest associations were identified between $A\beta$ plaques and other lesions such as CAA, tau, and LATE-NC. We also confirmed a close relationship between LATE-NC and amygdala-predominant α Syn. Experimental studies have demonstrated that $A\beta$ and αSyn can enhance tau seeding and aggregation, 14,15,55 while α Syn has also been implicated in the deposition and seeding of TDP-43 pathology. 15,19 Overall, extracellular A β accumulation and amygdala-predominant α Syn appear to have a less direct role in neuronal loss than pTau and LATE-NC, but may

15525279, 2025, 7, Downloaded from https:

enberg, Wiley Online Library on [15/10/2025]. See the Term

of use; OA articles are governed by the applicable Creative Comm

be crucial in facilitating the aggregation and propagation of these lesions.

Next, we investigated the role of APOE $\varepsilon 4$ in the network of neuropathologies. We confirmed a direct relationship between APOE $\varepsilon 4$ and extracellular A β deposition, as well as a strong association with CAA type 1 with capillary involvement. 34,56,57 In contrast, the general severity of CAA was not related to APOE $\varepsilon 4$ but showed a modest association with cognitive impairment and was linked not only to A β , but also to pTau and amygdala-predominant α Syn. These findings suggest distinct underlying mechanisms for CAA types 1 and 2. Moreover, they support the hypothesis that one of CAA's harmful effects is its role in exacerbating protein aggregation, for example, by stiffening blood vessels and restricting blood flow, thereby impairing perivascular clearance. 58,59

We found no evidence of a direct link between APOE $\varepsilon 4$ and Braak NFT staging. While mouse and cell models suggest that APOE $\varepsilon 4$ independently promotes pTau accumulation,⁶⁰ human studies align with our findings, showing no effect on pTau pathology after accounting for $A\beta$.⁶¹⁻⁶³ However, because Braak NFT staging is a broad measure of pTau spread there is still a possibility that APOE $\varepsilon 4$ is specifically associated with pTau burden in MTL regions, as suggested by some studies.⁶⁴ Additionally, we found no relationship between APOE $\varepsilon 4$ and amygdala-predominant α Syn, which contrasts with previous studies reporting that APOE $\varepsilon 4$ exacerbates α Syn pathology independently of $A\beta$.^{65,66} This may be due to our more rigorous adjustment for $A\beta$ lesions, or it could suggest that APOE $\varepsilon 4$ primarily influences other variants of α Syn.

Finally, we cannot rule out a potential association between APOE $\varepsilon 4$ and LATE-NC, as previously reported in the literature, ^{11,67} given that this relationship in our cohort approached statistical significance. However, further research is needed to clarify the relationship between LATE-NC, APOE $\varepsilon 4$, and A β , the latter of which showed an unexpectedly strong association with LATE-NC in our cohort. While previous studies have suggested that TDP-43 may inhibit A β fibrillization, resulting in the accumulation of toxic A β oligomers and increased neurotoxicity, ⁶⁸ this mechanism does not fully explain the observed LATE-NC association with overall A β burden.

We also systematically examined other pathologies that may contribute to global or hippocampal degeneration. Among cerebrovascular lesions, we found that SVD in the temporal white matter and atherosclerosis in the circle of Willis were both associated with CA1 neuron loss, aligning with previous findings. 23,28 The CA1 region is particularly vulnerable to hypoxic damage, ⁶⁹ and cerebrovascular lesions may contribute to neuronal loss by reducing blood flow.⁵⁹ However, in a comprehensive model, the association between SVD and CA1 damage appeared to be mediated by its links to LATE-NC and amygdala-predominant α Syn. While previous studies have established a connection between LATE-NC and SVD,53,70,71 the relationship between SVD and α Syn remains unclear and requires further investigation. Given that hypoxia has been shown to promote α Syn aggregation and enhance its toxicity,⁷² this link is biologically plausible. Moreover, SVD was associated with atherosclerosis and infarction, suggesting it may serve as a key mediator between cerebrovascular damage and the broader spectrum of AD neuropathology.

Interestingly, we found that Hirano bodies were positively associated with CA1 neuronal density, suggesting a potential protective role against hippocampal damage. These rod-shaped intracellular aggregates, primarily composed of actin, ⁷³ have been linked to neuropathological changes such as NFTs in AD. ⁷⁴ Consistent with our findings, studies using Hirano body models suggest that these inclusions may help reduce cell death associated with tau and the APP intracellular domain. ⁷⁵ However, further research is needed to clarify their function in neurodegenerative processes.

In contrast, other lesions, including ARTAG, AGD, hippocampal vascular calcifications, and multiple old infarctions, showed no clear association with hippocampal or global brain degeneration, nor did they exhibit any discernible trends. Despite its established link to LATE-NC, ARTAG showed no such relation in our analysis. Instead, in our cohort, ARTAG was associated only with temporal SVD, not with LATE-NC. AGD was not associated with any measures of brain degeneration and, unexpectedly, was negatively correlated with AD-related lesions. This finding contributes to the ongoing debate on whether AGD represents a distinct neuropathological disease or if these tau lesions are largely benign. 77,78

Neuronal density serves as a reliable marker of neurodegeneration and hippocampal atrophy, but manual counting is time consuming and affected by variability in staining techniques, anatomical sampling, and cell morphology. While algorithms exist for neuron quantification from Nissl staining,⁷⁹ this staining is incompatible with immunohistochemistry. To overcome this limitation, we developed a neuronal classifier for hematoxylin-stained slides. Its accuracy matches that of independent human raters, providing a reproducible and efficient approach for assessing pyramidal neuronal loss in large cohorts.

This study has several limitations. First, sample sizes varied across analyses. While core parameters were measured in all 480 cases, other measures (e.g., brain weight, CDR) were not available for the entire cohort. As a result, models based on incomplete samples may be underpowered. Additionally, our dataset lacks information on the education levels of the included cases, which could confound analyses involving the CDR. Therefore, results with this parameter should be interpreted with caution. Moreover, the structural equation modeling assumed unidirectional pathways, which may oversimplify the complex biological interactions between protein aggregates. Reciprocal interactions, such as those between A β and pTau or between TDP-43 and pTau, exist but were not fully captured. Notably, the α Syn → LATE-NC pathway had to be reversed to achieve model fit, even though this reversal does not align with the suspected biological directionality. Finally, the parameters used to estimate tau, $A\beta$, and LATE-NC were based on lesion distribution (i.e., staging schemes) rather than (semi)quantitative assessments. This approach may influence the results, as lesion spread may not fully reflect the local pathological burden.

Overall, our findings indicate that AD pathology extends beyond $A\beta$ and pTau, incorporating limbic-predominant variants of α Syn and TDP-43 pathologies, all of which contribute to brain degeneration. While pTau and LATE-NC were the strongest predictors of neuronal loss, $A\beta$ and α Syn may play an additional critical role by promoting the

aggregation and spread of other pathological proteins. These results underscore the need for improved in vivo detection of brain lesions to enhance patient stratification.

ACKNOWLEDGMENTS

The authors thank GE Healthcare for providing samples for this study and Petra Weckx for technical assistance. The authors appreciate Grzegorz Walkiewicz and Bas Moonen for their feedback on the content and figures. The authors also acknowledge Kamil Sekut for proposing the idea behind the machine-learning algorithm for neuron detection. Finally, the authors thank the patients and their families for their contributions. This study was supported by grants from the Fond Wetenschappelijk Onderzoek (FWO, Belgium): G0F8516N (DRT), G065721N, and G024925N (DRT, KS); KU Leuven Onderzoeksraad (Belgium): C14/17/107 (DRT), C14/22/132 (DRT), and C3/20/057 (DRT); Deutsche Forschungsgemeinschaft (DFG, Germany): TH-624-4-1, TH-624-4-2, TH-624-6-1 (DRT); Alzheimer Forschung Initiative (AFI, Germany): #10810, #13803 (DRT); and the Alzheimer's Association (USA): 22-AAIIA-963171 (DRT). SOT was supported by KU Leuven Internal Funding (PDMT2/21/069), the BrightFocus Foundation (A2022019F), Fonds Wetenschappelijk Onderzoek (1225725N), and the Alzheimer's Association (AARF-24-1300693). MO received support from the EU Joint Programme-Neurodegenerative Diseases network Genfi-Prox (01ED2008A), the German Federal Ministry of Education and Research (FTLDc 01GI1007A), the EU Moodmarker program (01EW2008), the German Research Foundation (DFG) (SFB1279), the Foundation of the State of Baden-Württemberg (D.3830), Boehringer Ingelheim Ulm University BioCenter (D.5009), the Thierry Latran Foundation (D.2468), and the Roux Program of the Martin Luther University Halle-Wittenberg.

CONFLICT OF INTEREST STATEMENT

DRT and SOT received consultant honoraria from Muna Therapeutics (Belgium). DRT collaborated with Novartis Pharma AG (Switzerland), and GE Healthcare (UK). CAFvA has received honoraria for serving on the scientific advisory board of Biogen, Roche, Novo Nordisk, BioNTech, Lilly, Dr Willmar Schwabe GmbH & Co.KG and MindAhead UG. Additionally, CAFvA has received travel funding and speaker honoraria from Biogen, Lilly, Novo Nordisk, Roche Diagnostics AG, Novartis, Medical Tribune Verlagsgesellschaft mbH, Landesvereinigung für Gesundheit und Akademie für Sozialmedizin Niedersachsen e. V., FomF GmbH | Forum für medizinische Fortbildung, and Dr Willmar Schwabe GmbH & Co.KG. Research support was received from Roche Diagnostics AG, and funding was provided by the Innovationsfond (Fund of the Federal Joint Committee, Gemeinsamer Bundesausschuss, G-BA; Grants No. VF1_2016-201; 01NVF21010; 01VSF21019). MO has provided scientific advice to Fujirebio, Roche, Biogen, Lilly, and Axon. RV's institution has clinical trial agreements (RV as PI) with Alector, AviadoBio, Biogen, Denali, J&J, Eli Lilly, and UCB. RV's institution has consultancy agreements (RV as member of DSMB) with AC Immune. All other authors had nothing to disclose. Author disclosures are available in the supporting information.

CONSENT STATEMENT

All human donors in the study were fully informed and provided their consent to participate in accordance with ethical guidelines and the laws of Belgium, Germany, and the UK. All experiments were conducted following ethical clearance from the Ethics Committee Research UZ / KU Leuven (identifier: \$65147).

DATA AVAILABILITY STATEMENT

The raw data used in this study are publicly available in Table \$18 in supporting information. The Python package implementing the neuron detection algorithm for hematoxylin-stained slides is publicly available at https://github.com/neuropathology-lab/neurodetection.

ORCID

Klara Gawor https://orcid.org/0000-0001-7571-5420 Sam Verrept https://orcid.org/0009-0001-0918-7890 Geethika Arekatla https://orcid.org/0009-0002-2639-9964 David Wouters https://orcid.org/0000-0002-8000-8023 Alicia Ronisz https://orcid.org/0000-0002-4310-0445 Celeste Laurevssen https://orcid.org/0000-0002-7373-2099 Bas Lahaije https://orcid.org/0009-0001-5887-6844 Christine A. F. von Arnim https://orcid.org/0000-0002-8614-2223 Bernard Hanseeuw https://orcid.org/0000-0002-3102-6778 Rik Vandenberghe https://orcid.org/0000-0001-6237-2502 Matthew Blaschko https://orcid.org/0000-0002-2640-181X Alejandro Sifrim https://orcid.org/0000-0001-8247-4020 Kristel Sleegers https://orcid.org/0000-0002-0283-2332 Dietmar Rudolf Thal https://orcid.org/0000-0002-1036-1075 Sandra O. Tomé https://orcid.org/0000-0001-5253-0730

REFERENCES

- 1. Montine TJ, Phelps CH, Beach TG, et al. National Institute on Aging-Alzheimer's Association guidelines for the neuropathologic assessment of Alzheimer's disease: a practical approach. Acta Neuropathol. 2012;123(1):1-11. doi:10.1007/s00401-011-0910-3
- 2. Braak H, Braak E. Neuropathological stageing of Alzheimerchanges. Acta Neuropathol. 1991;82(4):239-259. related doi:10.1007/BF00308809
- 3. Thal DR, Rüb U, Orantes M, Braak H. Phases of Aβ -deposition in the human brain and its relevance for the development of AD. Neurology. 2002;58(12):1791-1800. doi:10.1212/wnl.58.12.1791
- 4. Nichols E, Merrick R, Hay SI, et al. The prevalence, correlation, and co-occurrence of neuropathology in old age: harmonisation of 12 measures across six community-based autopsy studies of dementia. The Lancet Healthy Longevity. 2023;4(3):e115-e125. doi:10.1016/S2666-7568(23)00019-3
- 5. Jellinger KA. Pathobiological subtypes of Alzheimer disease. Dement Geriatr Cogn Disord. 2021;49(4):321-333. doi:10.1159/000508625
- 6. Robinson JL, Richardson H, Xie SX, et al. The development and convergence of co-pathologies in Alzheimer's disease. Brain. 2021;144(3):953-962. doi:10.1093/brain/awaa438
- 7. Aggleton JP. Multiple anatomical systems embedded within the primate medial temporal lobe: implications for hippocampal function. Neurosci Biobehav Rev. 2012;36(7):1579-1596. doi:10.1016/j. neubiorev.2011.09.005
- 8. Jack CR, Petersen RC, Xu YC, et al. Medial temporal atrophy on MRI in normal aging and very mild Alzheimer's disease. Neurology. 1997;49(3):786-794. doi:10.1212/WNL.49.3.786

- Nelson PT, Dickson DW, Trojanowski JQ, et al. Limbic-predominant age-related TDP-43 encephalopathy (LATE): consensus working group report. Brain. 2019;142(6):1503-1527. doi:10.1093/brain/awz099
- 10. Toledo JB, Gopal P, Raible K, et al. Pathological α -synuclein distribution in subjects with coincident Alzheimer's and Lewy body pathology. *Acta Neuropathol.* 2016;131(3):393-409. doi:10.1007/s00401-015-1526-0
- Josephs KA, Whitwell JL, Weigand SD, et al. TDP-43 is a key player in the clinical features associated with Alzheimer's disease. Acta Neuropathol. 2014;127(6):811-824. doi:10.1007/s00401-014-1269-z
- Raunio A, Kaivola K, Tuimala J, et al. Lewy-related pathology exhibits two anatomically and genetically distinct progression patterns: a population-based study of Finns aged 85. Acta Neuropathol. 2019;138(5):771-782. doi:10.1007/s00401-019-02071-3
- Uchikado H, Lin WL, DeLucia MW, Dickson DW. Alzheimer Disease With Amygdala Lewy Bodies: a Distinct Form of α-Synucleinopathy. J Neuropathol Exp Neurol. 2006;65(7):685-697. doi:10.1097/01.jnen. 0000225908.90052.07
- Götz J, Chen F, van Dorpe J, Nitsch RM. Formation of neurofibrillary tangles in P301l tau transgenic mice induced by Abeta 42 fibrils. Science. 2001;293(5534):1491-1495. doi:10.1126/science.1062097
- Nonaka T, Masuda-Suzukake M, Hasegawa M. Molecular mechanisms of the co-deposition of multiple pathological proteins in neurodegenerative diseases. *Neuropathology*. 2018;38(1):64-71. doi:10.1111/ neup.12427
- 16. Gawor K, Tomé SO, Vandenberghe R, et al. Amygdala-predominant α -synuclein pathology is associated with exacerbated hippocampal neuron loss in Alzheimer's disease. *Brain Commun.* 2024;6(6):fcae442. doi:10.1093/braincomms/fcae442
- 17. Tomé SO, Gomes LA, Li X, Vandenberghe R, Tousseyn T, Thal DR. TDP-43 interacts with pathological τ protein in Alzheimer's disease. *Acta Neuropathol.* 2021;141(5):795-799. doi:10.1007/s00401-021-02295-2
- Higashi S, Iseki E, Yamamoto R, et al. Concurrence of TDP-43, tau and α-synuclein pathology in brains of Alzheimer's disease and dementia with Lewy bodies. *Brain Res.* 2007;1184:284-294. doi:10.1016/j. brainres.2007.09.048
- Dhakal S, Wyant CE, George HE, Morgan SE, Rangachari V. Prion-like C-Terminal Domain of TDP-43 and α-Synuclein Interact Synergistically to Generate Neurotoxic Hybrid Fibrils. *J Mol Biol*. 2021;433(10):166953. doi:10.1016/j.jmb.2021.166953
- Josephs KA, Murray ME, Tosakulwong N, et al. Tau aggregation influences cognition and hippocampal atrophy in the absence of betaamyloid: a clinico-imaging-pathological study of primary age-related tauopathy (PART). Acta Neuropathol. 2017;133(5):705-715. doi:10. 1007/s00401-017-1681-2
- Krantic S, Isorce N, Mechawar N, et al. Hippocampal GABAergic neurons are susceptible to amyloid-β toxicity in vitro and are decreased in number in the Alzheimer's disease TgCRND8 mouse model. J Alzheimers Dis. 2012;29(2):293-308. doi:10.3233/JAD-2011-110830
- Ferrer I, Santpere G, van Leeuwen FW. Argyrophilic grain disease. Brain. 2008;131(6):1416-1432. doi:10.1093/brain/awm305
- Sordo L, Qian T, Bukhari SA, et al. Characterization of hippocampal sclerosis of aging and its association with other neuropathologic changes and cognitive deficits in the oldest-old. *Acta Neuropathol*. 2023;146(3):415-432. doi:10.1007/s00401-023-02606-9
- Koper MJ, Tomé SO, Gawor K, et al. LATE-NC aggravates GVD-mediated necroptosis in Alzheimer's disease. Acta Neuropathol Commun. 2022;10(1):128. doi:10.1186/s40478-022-01432-6
- Furgerson M, Clark JK, Crystal JD, Wagner JJ, Fechheimer M, Furukawa R. Hirano body expression impairs spatial working memory in a novel mouse model. *Acta Neuropathologica Communications*. 2014;2(1):131. doi:10.1186/s40478-014-0131-9
- Nagaraja N, Wang WE, Duara R, DeKosky ST, Vaillancourt D. Mediation of Reduced Hippocampal Volume by Cerebral Amyloid Angiopa-

- thy in Pathologically Confirmed Patients with Alzheimer's Disease. *J Alzheimers Dis.* 2023;93(2):495-507. doi:10.3233/JAD-220624
- Wegiel J, Kuchna I, Wisniewski T, et al. Vascular fibrosis and calcification in the hippocampus in aging, Alzheimer disease, and Down syndrome. *Acta Neuropathol.* 2002;103(4):333-343. doi:10.1007/s00401-001-0471-y
- 28. Kapasi A, Capuano AW, Lamar M, et al. Atherosclerosis and Hippocampal Volumes in Older Adults: the Role of Age and Blood Pressure. *J Am Heart Assoc.* 2024;13(3):e031551. doi:10.1161/JAHA.123.031551
- Hatters DM, Peters-Libeu CA, Weisgraber KH. Apolipoprotein E structure: insights into function. *Trends Biochem Sci.* 2006;31(8):445-454. doi:10.1016/j.tibs.2006.06.008
- Jackson RJ, Hyman BT, Serrano-Pozo A. Multifaceted roles of APOE in Alzheimer disease. Nat Rev Neurol. 2024;20(8):457-474. doi:10.1038/ s41582-024-00988-2
- Beecham GW, Hamilton K, Naj AC, et al. Genome-wide association meta-analysis of neuropathologic features of Alzheimer's disease and related dementias. PLoS Genet. 2014;10(9):e1004606. doi:10.1371/ journal.pgen.1004606
- Shade LMP, Katsumata Y, Abner EL, et al. GWAS of multiple neuropathology endophenotypes identifies new risk loci and provides insights into the genetic risk of dementia. *Nat Genet*. 2024;56(11):2407-2421. doi:10.1038/s41588-024-01939-9
- Laureyssen C, Küçükali F, Van Dongen J, et al. Hypothesis-based investigation of known AD risk variants reveals the genetic underpinnings of neuropathological lesions observed in Alzheimer's-type dementia.
 Acta Neuropathol. 2024;148(1):55. doi:10.1007/s00401-024-02815-w
- Wisniewski T, Drummond E. APOE-amyloid interaction: therapeutic targets. Neurobiol Dis. 2020;138:104784. doi:10.1016/j.nbd.2020. 104784
- Hughes CP, Berg L, Danziger WL, Coben LA, Martin RL. A new clinical scale for the staging of dementia. Br J Psychiatry. 1982;140:566-572. doi:10.1192/bjp.140.6.566
- Arevalo-Rodriguez I, Smailagic N, Roqué I, Figuls M, et al. Mini-Mental State Examination (MMSE) for the detection of Alzheimer's disease and other dementias in people with mild cognitive impairment (MCI). Cochrane Database Syst Rev. 2015;2015(3):CD010783. doi:10.1002/ 14651858.CD010783.pub2
- Perneczky R, Wagenpfeil S, Komossa K, Grimmer T, Diehl J, Kurz A. Mapping scores onto stages: mini-mental state examination and clinical dementia rating. Am J Geriatr Psychiatry. 2006;14(2):139-144. doi:10.1097/01.JGP.0000192478.82189.a8
- Larionov S, Dedeck O, Birkenmeier G, Orantes M, Ghebremedhin E, Thal DR. The intronic deletion polymorphism of the Alpha2-macroglobulin gene modulates the severity and extent of atherosclerosis in the circle of Willis. *Neuropathol Appl Neurobiol*. 2006;32(4):451-454. doi:10.1111/j.1365-2990.2006.00743.x
- Mirra SS, Heyman A, McKeel D, et al. The Consortium to Establish a Registry for Alzheimer's Disease (CERAD). Part II. Standardization of the neuropathologic assessment of Alzheimer's disease. *Neurology*. 1991;41(4):479-486. doi:10.1212/wnl.41.4.479
- Thal DR, Ghebremedhin E, Rüb U, Yamaguchi H, Del Tredici K, Braak H. Two types of sporadic cerebral amyloid angiopathy. J Neuropathol Exp Neurol. 2002;61(3):282-293. doi:10.1093/jnen/61.3.282
- Vonsattel JP, Myers RH, Hedley-Whyte ET, Ropper AH, Bird ED, Richardson EP. Cerebral amyloid angiopathy without and with cerebral hemorrhages: a comparative histological study. *Ann Neurol*. 1991;30(5):637-649. doi:10.1002/ana.410300503
- Alafuzoff I, Thal DR, Arzberger T, et al. Assessment of beta-amyloid deposits in human brain: a study of the BrainNet Europe Consortium. Acta Neuropathol. 2009;117(3):309-320. doi:10.1007/s00401-009-0485-4
- 43. Alafuzoff I, Pikkarainen M, Arzberger T, et al. Inter-laboratory comparison of neuropathological assessments of beta-amyloid

- 44. Kovacs GG, Ferrer I, Grinberg LT, et al. Aging-related tau astrogliopathy (ARTAG): harmonized evaluation strategy. Acta Neuropathol. 2016:131(1):87-102. doi:10.1007/s00401-015-1509-x
- 45. Braak H, Braak E. Argyrophilic grain disease: frequency of occurrence in different age categories and neuropathological diagnostic criteria. J Neural Transm (Vienna). 1998;105(8-9):801-819. doi:10.1007/ s007020050096
- 46. Nelson PT, Lee EB, Cykowski MD, et al. LATE-NC staging in routine neuropathologic diagnosis: an update. Acta Neuropathol. 2023;145(2):159-173. doi:10.1007/s00401-022-02524-2
- 47. Thal DR, Del Tredici K, Ludolph AC, et al. Stages of granulovacuolar degeneration: their relation to Alzheimer's disease and chronic stress response. Acta Neuropathol. 2011;122(5):577-589. doi:10. 1007/s00401-011-0871-6
- 48. Rubinacci S, Ribeiro DM, Hofmeister RJ, Delaneau O. Efficient phasing and imputation of low-coverage sequencing data using large reference panels. Nat Genet. 2021;53(1):120-126. doi:10.1038/s41588-020-00756-0
- 49. Hixson JE, Vernier DT. Restriction isotyping of human apolipoprotein E by gene amplification and cleavage with Hhal. J Lipid Res. 1990:31(3):545-548.
- 50. Karanth S, Nelson PT, Katsumata Y, et al. Prevalence and Clinical Phenotype of Quadruple Misfolded Proteins in Older Adults. JAMA Neurol. 2020;77(10):1299-1307. doi:10.1001/jamaneurol.2020.1741
- 51. Tomé SO, Tsaka G, Ronisz A, et al. TDP-43 pathology is associated with increased tau burdens and seeding. Mol Neurodegener. 2023;18(1):71. doi:10.1186/s13024-023-00653-0
- 52. Agrawal S, Yu L, Leurgans SE, et al. Hippocampal neuronal loss and cognitive decline in LATE-NC and ADNC among community-dwelling older persons. Alzheimers Dement. 2025:e14500. doi:10.1002/alz. 14500. Published online January 30.
- 53. Mikhailenko E, Colangelo K, Tuimala J, et al. Limbic-predominant age-related TDP-43 encephalopathy in the oldest old: a populationbased study. Brain. 2025;148(1):154-167. doi:10.1093/brain/ awae212
- 54. Wisse LEM, Wuestefeld A, Murray ME, Jagust W. Role of tau versus TDP-43 pathology on medial temporal lobe atrophy in aging and Alzheimer's disease. Alzheimers Dement. 2025;21(2):e14582. doi:10. 1002/alz.14582
- 55. Bassil F, Brown HJ, Pattabhiraman S, et al. Amyloid-Beta (A β) Plaques Promote Seeding and Spreading of Alpha-Synuclein and Tau in a Mouse Model of Lewy Body Disorders with A\beta Pathology. Neuron. 2020;105(2):260-275. doi:10.1016/j.neuron.2019.10.010. e6.
- 56. Thal DR, Papassotiropoulos A, Saido TC, et al. Capillary cerebral amyloid angiopathy identifies a distinct APOE epsilon4-associated subtype of sporadic Alzheimer's disease. Acta Neuropathol. 2010;120(2):169-183. doi:10.1007/s00401-010-0707-9
- 57. Yu L, Boyle PA, Nag S, et al. APOE and Cerebral Amyloid Angiopathy in Community Dwelling Older Persons. Neurobiol Aging. 2015;36(11):2946-2953. doi:10.1016/j.neurobiolaging.2015.08.008
- 58. van Veluw SJ, Benveniste H, Bakker ENTP, et al. Is CAA a perivascular brain clearance disease? A discussion of the evidence to date and outlook for future studies. Cell Mol Life Sci. 2024;81(1):239. doi:10.1007/ s00018-024-05277-1
- 59. Thal DR, Grinberg LT, Attems J. Vascular dementia: different forms of vessel disorders contribute to the development of dementia in the elderly brain. Exp Gerontol. 2012;47(11):816-824. doi:10.1016/j.exger. 2012.05.023
- 60. Harris FM, Brecht WJ, Xu Q, Mahley RW, Huang Y. Increased tau phosphorylation in apolipoprotein E4 transgenic mice is associated with activation of extracellular signal-regulated kinase: modulation by zinc. J Biol Chem. 2004;279(43):44795-44801. doi:10.1074/jbc. M408127200

- 61. Cicognola C. Salvadó G. Smith R. et al. APOE4 impact on soluble and insoluble tau pathology is mostly influenced by amyloid-beta. Brain. Published online January 16, 2025; awaf016. doi:10.1093/brain/ awaf016
- 62. Farfel JM, Yu L, De Jager PL, Schneider JA, Bennett DA. Association of APOE with tau-tangle pathology with and without β -amyloid. Neurobiol Aging. 2016;37:19-25. doi:10.1016/j.neurobiolaging.2015.09.011
- 63. Morris JC, Roe CM, Xiong C, et al. APOE predicts amyloid-beta but not tau Alzheimer pathology in cognitively normal aging. Ann Neurol. 2010;67(1):122-131. doi:10.1002/ana.21843
- 64. Young CB, Johns E, Kennedy G, et al. APOE effects on regional tau in preclinical Alzheimer's disease. Molecular Neurodegeneration. 2023;18(1). doi:10.1186/s13024-022-00590-4
- 65. Zhao N, Attrebi ON, Ren Y, et al. APOE4 exacerbates α -synuclein pathology and related toxicity independent of amyloid. Sci Transl Med. 2020;12(529):eaay1809. doi:10.1126/scitranslmed.aay1809
- 66. Dickson DW, Heckman MG, Murray ME, et al. APOE ε4 is associated with severity of Lewy body pathology independent of Alzheimer pathology. Neurology. 2018;91(12):e1182-e1195. doi:10.1212/WNL. 0000000000006212
- 67. Dugan AJ, Nelson PT, Katsumata Y, et al. Analysis of genes (TMEM106B, GRN, ABCC9, KCNMB2, and APOE) implicated in risk for LATE-NC and hippocampal sclerosis provides pathogenetic insights: a retrospective genetic association study. Acta Neuropathologica Communications. 2021;9(1):152. doi:10.1186/s40478-021-01250-
- 68. Shih YH, Tu LH, Chang TY, et al. TDP-43 interacts with amyloid-β, inhibits fibrillization, and worsens pathology in a model of Alzheimer's disease. Nat Commun. 2020;11(1):5950. doi:10.1038/s41467-020-19786-7
- 69. Sadowski M, Wisniewski HM, Jakubowska-Sadowska K, Tarnawski M, Lazarewicz JW, Mossakowski MJ. Pattern of neuronal loss in the rat hippocampus following experimental cardiac arrest-induced ischemia. J Neurol Sci. 1999;168(1):13-20. doi:10.1016/S0022-510X(99)00159-
- 70. Nelson PT, Katsumata Y. Arteriolosclerosis and LATE-NC: two common and inter-related contributors to Alzheimer's-type dementia. Alzheimers Dement. 2025;20(Suppl 1):e085805. doi:10.1002/alz.
- 71. Harrison WT, Lusk JB, Liu B, et al. Limbic-predominant age-related TDP-43 encephalopathy neuropathological change (LATE-NC) is independently associated with dementia and strongly associated with arteriolosclerosis in the oldest-old. Acta Neuropathol. 2021;142(5):917-919. doi:10.1007/s00401-021-02360-w
- 72. Burtscher J, Syed MMK, Keller MA, Lashuel HA, Millet GP. Fatal attraction-The role of hypoxia when alpha-synuclein gets intimate with mitochondria. Neurobiol Aging. 2021;107:128-141. doi:10.1016/ j.neurobiolaging.2021.07.017
- 73. Hirano A. Hirano bodies and related neuronal inclusions. Neuropathol Appl Neurobiol. 1994;20(1):3-11. doi:10.1111/j.1365-2990. 1994.tb00951.x
- 74. Yoshida K, Forrest SL, Ichimata S, et al. Revisiting the relevance of Hirano bodies in neurodegenerative diseases. Neuropathol Appl Neurobiol. 2024;50(2):e12978. doi:10.1111/nan.12978
- 75. Spears W, Furgerson M, Sweetnam JM, et al. Hirano bodies differentially modulate cell death induced by tau and the amyloid precursor protein intracellular domain. BMC Neurosci. 2014;15:74. doi:10.1186/ 1471-2202-15-74
- 76. Katsumata Y, Wu X, Aung KZ, et al. Pathologic correlates of agingrelated tau astrogliopathy: aRTAG is associated with LATE-NC and cerebrovascular pathologies, but not with ADNC. Neurobiol Dis. 2024;191:106412. doi:10.1016/j.nbd.2024.106412
- 77. Grinberg LT, Heinsen H. Argyrophilic grain disease: an update about a frequent cause of dementia. Dement Neuropsychol. 2009;3(1):2-7. doi:10.1590/S1980-57642009DN30100002

- 78. Jellinger KA. Dementia with grains (argyrophilic grain disease). *Brain Pathol.* 1998;8(2):377-386. doi:10.1111/j.1750-3639.1998.tb00161.
- Oltmer J, Rosenblum EW, Williams EM, et al. Stereology neuron counts correlate with deep learning estimates in the human hippocampal subregions. Sci Rep. 2023;13(1):5884. doi:10.1038/s41598-023-32903-y

SUPPORTING INFORMATION

Additional supporting information can be found online in the Supporting Information section at the end of this article.

How to cite this article: Gawor K, Verrept S, Arekatla G, et al. Alzheimer's disease and its co-pathologies: Implications for hippocampal degeneration, cognitive decline, and the role of APOE $\varepsilon 4$. Alzheimer's Dement. 2025;21:e70483.

https://doi.org/10.1002/alz.70483